



LAWRENCE
LIVERMORE
NATIONAL
LABORATORY

Isotope-specific detection of low density materials with mono-energetic (gamma)-rays

F. Albert, S. G. Anderson, D. J. Gibson, C. A. Hagmann, M. S. Johnson, M. J. Messerly, V. A. Semenov, M. Y. Shverdin, A. M. Tremaine, F. V. Hartemann, C. W. Siders, D. P. McNabb, C. P. J. Barty

March 18, 2009

Disclaimer

This document was prepared as an account of work sponsored by an agency of the United States government. Neither the United States government nor Lawrence Livermore National Security, LLC, nor any of their employees makes any warranty, expressed or implied, or assumes any legal liability or responsibility for the accuracy, completeness, or usefulness of any information, apparatus, product, or process disclosed, or represents that its use would not infringe privately owned rights. Reference herein to any specific commercial product, process, or service by trade name, trademark, manufacturer, or otherwise does not necessarily constitute or imply its endorsement, recommendation, or favoring by the United States government or Lawrence Livermore National Security, LLC. The views and opinions of authors expressed herein do not necessarily state or reflect those of the United States government or Lawrence Livermore National Security, LLC, and shall not be used for advertising or product endorsement purposes.

This work performed under the auspices of the U.S. Department of Energy by Lawrence Livermore National Laboratory under Contract DE-AC52-07NA27344.

Isotope-specific detection of low density materials with mono-energetic γ -rays

F. Albert, S.G. Anderson, D.J. Gibson, C.A. Hagmann, M.S. Johnson, M.J. Messerly, V.A. Semenov, M.Y. Shverdin, A.M. Tremaine, F.V. Hartemann, C.W. Siders, D.P. McNabb and C.P.J. Barty
Lawrence Livermore National Laboratory, 7000 East Avenue, Livermore, CA, 94550

The first demonstration of isotope-specific detection of a low-Z, low density object, shielded by a high-Z and high density material using mono-energetic gamma-rays is reported. Isotope-specific detection of LiH shielded by Pb and Al is accomplished using the nuclear resonance fluorescence line of ${}^7\text{Li}$ at 0.478 MeV. Resonant photons are produced via laser-based Compton scattering. The detection techniques are general and the confidence level obtained is shown to be superior to that yielded by conventional x-ray/ γ -ray techniques in these situations.

PACS numbers: 41.60.Ap, 07.85.Fv, 42.55.Wd, 25.20.Dc

In this Letter, we report what we believe to be the first demonstration of a general technique that will enable the detection and identification of low-Z, low density targets, shielded by high-Z and high density materials. We describe the detection of a LiH target, shielded by Pb and Al using Nuclear Resonance Fluorescence (NRF) and LLNL's T-REX (Thomson-Radiated Extreme X-rays) mono-energetic γ -ray source. T-REX is a laser-based source that produces mono-energetic, tunable, polarized γ -rays via Compton scattering of energetic short duration laser pulses from high-brightness relativistic electron bunches. While the results presented here correspond to a proof-of-principle experiment, the range of applications for this new "inverse density" detection capability is quite broad and includes special nuclear material detection [1], stockpile surveillance [2], nuclear waste assay [3], medical imaging and industrial non-destructive evaluation.

The detection of low-Z, low-density objects shielded by high-Z, dense material is a long-standing problem that has important applications ranging from homeland security and non-proliferation [4] to advanced biomedical imaging and paleontology. X-rays are sensitive to electron density and x-ray radiography yields poor contrast in these situations. Within this context, NRF offers a unique approach to the so-called inverse density radiography problem. NRF is a process in which nuclei are excited by discrete high-energy (typically MeV) photons and subsequently re-emit γ -rays at discrete energies determined by the structure of the nucleus. Because the resonance structure is determined by the number of neutrons and protons present in the nucleus, NRF can provide isotope specific detection and imaging capability [5]. NRF has been recently used to detect shielded, dense, high-Z materials, such as ${}^{235}\text{U}$ or ${}^{239}\text{Pu}$, with a 4 MeV bremsstrahlung source [6].

NRF transitions are narrow band ($\Delta E/E \simeq 10^{-6}$); thus monochromatic Compton-scattering sources are favorable for that type of application when compared with Bremsstrahlung sources. Since Bremsstrahlung sources have 100% bandwidth, they create considerable background via elastic Compton scattering and other processes. Furthermore, the dose accumulated during detection is much higher than for a Compton source. A rel-

atively recent achievement of laser-based Compton scattering light sources is their high peak brightness at MeV energies [7, 8], a range that is beyond 3rd generation synchrotrons. Laser-based Compton scattering source development has been motivated by the desire to produce either sub-ps pulse duration x-rays for dynamic studies [9–11] or tunable radiation in the 10 keV–100 keV range for specific radiographic applications [12]. Recently, laser-based Compton γ -ray sources have been developed and used for nuclear science purposes: HI γ S, a 0.7–50 MeV high intensity γ -ray facility producing polarized photons via intra-cavity Compton backscattering in a free-electron laser, has been used as a research tool to assign the parity of excited states in nuclei using NRF [8], and ${}^{208}\text{Pb}$ has been detected in an iron box by using γ -rays produced by the collision of a Q-switched laser beam and a high energy electron beam from a storage ring [13].

Our experiment was performed at the LLNL linac facility, which houses a 120 MeV S-band linac and custom laser systems designed specifically for laser-based Compton scattering x-ray and γ -ray sources. The accelerator has been upgraded from previous laser Compton experiments [10, 11] to increase the electron beam brightness and energy. The experiments were conducted in three different below-ground caves: the outer detector cave, where the Interaction Laser System (ILS), producing the colliding photon beam was located; the accelerator cave, containing the photo-injector, the linac and the interaction region; and finally the 0° cave, on the other side of a thick concrete wall where the γ -ray diagnostics, including Ge detectors, were setup. A full description of the system can be found in Ref.[14]

The electron beam line begins at the photo-cathode, which consists of a Cu back plane on which a 2 μm thick sputter-coated layer of Mg has been deposited within a 1 cm diameter circle in the center. The high quantum efficiency of Mg enables the use of a fiber-based Photoinjector Drive Laser system (PDL) similar to [15]. The fiber system is seeded by an ultrafast 200 pJ, 75 fs fiber oscillator. Pulses from the oscillator are stretched and spectrally narrowed to 8 nm by a fiber Bragg grating [16] and amplified in a chain of fiber-based amplifiers to an

energy of 100 μJ at 10 kHz of 1053 nm. The pulses are further amplified by a bulk-optic regenerative amplifier to an energy of 1 mJ at 10 Hz. The pulses are then compressed by a bulk, dielectric-coated diffraction grating to 1 ps, frequency-quadrupled, sent through a pulse-stacking Hyper-Michelson interferometer [17] to produce a 15 ps flat-top temporal profile, apertured to produce a flat spatial profile, and finally relay-imaged to the photocathode, on which the incident UV laser energy is 30 μJ . The 0.5 nC, 5.5 MeV, 2 mm.mrad normalized emittance electron beam from the photo-cathode is coupled into the S-band linac, where it is accelerated by five 2.5 m SLAC-type traveling-wave sections up to 120 MeV, with a final normalized emittance of 5-6 mm.mrad.

The laser oscillator also serves as a seed for the Interaction Laser System (ILS), which also relies on chirped pulse amplification [18]. The pulse is first stretched and spectrally narrowed through a chirped fiber Bragg grating; then amplified by a series of fiber-based pre-amplifiers to 30 μJ at 10 kHz, and further amplified by a three head Nd:YAG power amplifier which delivers 750 mJ in 25 ps, 0.2 nm wide pulses centered at 1064 nm at a repetition rate of 10 Hz. The laser pulse is then compressed by a novel dielectric grating-based hyperdispersion pulse compressor [19], frequency-doubled with a DKPD crystal to yield 150 mJ at 532 nm, and focused inside a vacuum chamber (10^{-8} Torr) by a 2.4 m focal length $f/50$ lens down to 75 μm (full width at half maximum). For the 180° interaction geometry, the longitudinal position of the interaction region is set by the laser focus and the $35 \times 40 \mu\text{m}^2$ (*rms*) quadrupole-focussed electron beam. Optical transition radiation from the electron beam and reflection from the laser light on the cube can be imaged by a CCD for the spatial overlap and by a 2 ps resolution streak camera for the temporal overlap.

The measured spatial and spectral properties of the source, shown in Fig.1, are consistent with Compton scattering theory: the beam is collimated and the on-axis spectrum is sharply peaked and relatively narrow-band. The on-axis spectrum is peaked at an energy of $4\gamma^2 E_L$, where γ is the electron relativistic factor and E_L the laser photon energy. The beam profile has been measured with a 16 bit 1024×1024 pixels Intensified Charge Coupled Device (ICCD) Andor camera coupled to a 3:1 optical fiber reducer. The latter provides a $4 \times 4 \text{ cm}^2$ detection surface and is also coupled to a 140 μm CsI(Tl) scintillator which converts the γ -rays into green light. The whole system is protected from laser light with a 0.5 mm thick Be window and has been calibrated with a 662 keV ^{137}Cs radioisotope source. The 15 s (150 shots) beam profile shown in Fig. 1 indicates a $6.0 \times 10.4 \text{ mrad}^2$ divergence and an integrated x-ray dose of 10^5 photons/shot. The divergence is lower along the horizontal direction due to polarization effects [20]. The source spectrum has been measured through a 6 mm Pb collimator indirectly by scattering the γ -rays off a 3 mm thick Al plate onto a 50% efficiency, 2.8 keV resolution at 662 keV High Purity Germanium detector (HPGe) (with a $6 \times 8 \text{ cm}$ cylindrical

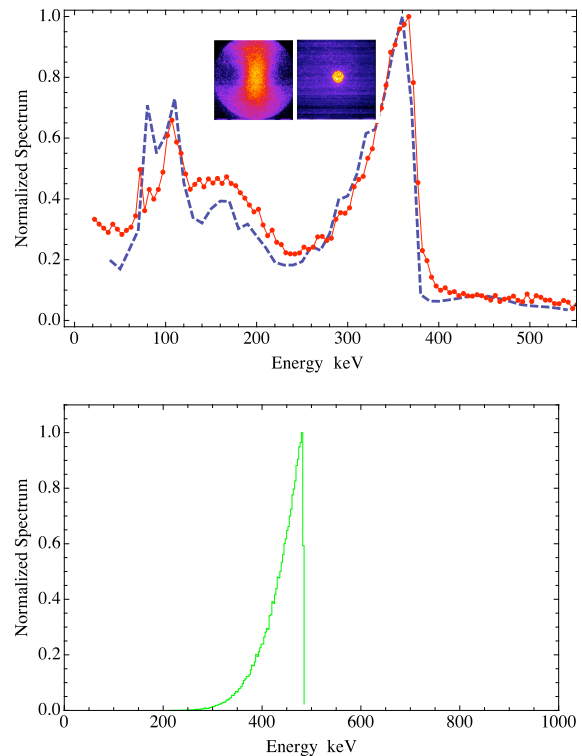


FIG. 1: Top: Experimentally measured on-axis spectra (dots) after scattering off the 3 mm Al plate for an electron beam energy of 116 MeV and corresponding Monte-Carlo simulation (dashed curve). The images represent the full beam profile and the collimator shadow on the ICCD (see details in text). Bottom: Input raw spectrum used in the Monte-Carlo simulation

Ge crystal) operating in a statistical single photon counting mode (rate of 20%), and placed 150 cm away from the plate. The scattered γ -rays of energy E'_γ are correlated to the incident γ -rays of energy E_γ by the Compton scattering relation $E'_\gamma = E_\gamma / [1 + E_\gamma / E_0 (1 - \cos \theta)]$, where $E_0 = 0.511 \text{ MeV}$ is the electron rest energy and $\theta = 48^\circ$ is the scattering angle of the γ -rays on the detector. The spectrum peaks at 365 keV (incident energy 478 keV) with a 15% relative bandwidth, which agrees with the results of the Monte-Carlo simulations from the MCNP5 code [21], plotted on top of the experimental spectrum in Fig. 1. The continuum below 250 keV is due to incomplete energy absorption (elastic Compton scattering) in the detector. The peak at 110 keV arises from double Compton scattering off the Al plate and the adjacent wall, followed by photo-absorption in the Ge detector. The peak near 88 keV is from x-ray fluorescence in the Pb shield surrounding the Ge detector. The tunability of the source has also been verified by measuring the γ -ray energy for additional electron beam energies of 68 MeV, 85 MeV and 101 MeV. The results are consistent with the Compton scattering for-

mula [22]. All the source parameters described above are summarized by the peak brightness at 478 keV, 1.5×10^{15} photons/mm²/mrad²/s/0.1%bandwidth. Higher brightness can be obtained by a combination of higher electron beam brightness and laser intensity.

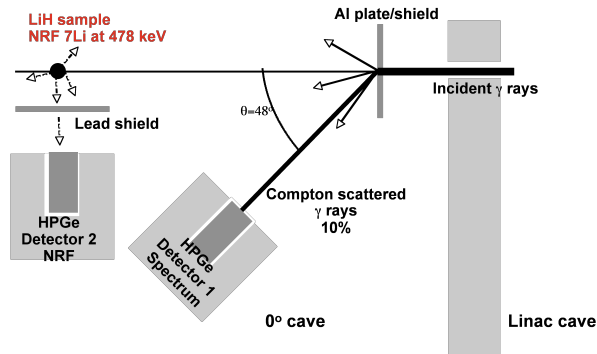


FIG. 2: Experimental setup for NRF detection in ${}^7\text{Li}$.

T-REX photons have been used to detect ${}^7\text{Li}$ with NRF by employing two methods. First we directly observe the scattered NRF photons. Second we observe the resonant attenuation of γ -rays in the transmitted beam to determine the presence or absence of the target material.

In a first experiment, the source has been used to detect the 0.478 MeV line of ${}^7\text{Li}$ ($Z_{\text{Li}}=3$) in a low density ($\rho_{\text{LiH}}=0.36$ g/cm³) LiH sample shielded by higher Z elements: 3 mm of Al ($Z_{\text{Al}}=13$) and 8 mm of Pb ($Z_{\text{Pb}}=82$). The ratio $\mu\rho_{\text{Pb}}/\mu\rho_{\text{LiH}}$, where μ is the mass attenuation coefficient, is equal to $\simeq 60$. 225 grams of LiH are placed in a light plastic bottle with a diameter of 8 cm, and are irradiated by the γ -ray beam, 20 m away from the source. At this location, the beam diameter, limited by the aperture along the beam path, is 4 cm. The experiment, depicted in Fig. 2, uses an additional HPGe detector. The source spectrum is monitored by the first HPGe to ensure a proper tuning of the γ -rays peak energy at 0.478 MeV. The NRF-scattered photons are detected by the second HPGe detector, positioned at 90° with respect to the incident beam axis and 15 cm away from the center of the beam. With the source parameters described above, NRF photons are expected to be scattered in a dipole radiation pattern at a rate of 16 photons/hour. The HPGe detector was positioned in the x-ray polarization plane to maximize the NRF signal from the M1 transition in ${}^7\text{Li}$ [23]. A scattering angle of 90° was chosen in order to minimize the amount of elastic Compton scattering background from the LiH target [24], since the γ -rays are linearly polarized. The count rate on the HPGe was close to 10% to avoid pile-up.

NRF data were acquired for 7.5 hours at 10 Hz and the results are shown in Fig. 3. The raw data (0.2 keV/channel) are binned to 1 keV resolution. The peak observed at 511 keV results from annihilation of e^+e^- pairs created by the high energy Bremsstrahlung from

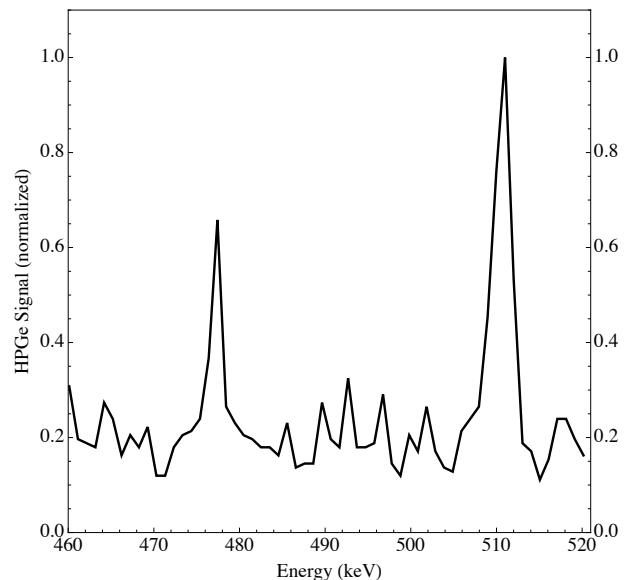


FIG. 3: Experimental results for NRF detection in ${}^7\text{Li}$. The black solid curve represents detected γ -ray photons scattered from the LiH sample.

the linac. This line is still present when the interaction laser is off. The NRF line from ${}^7\text{Li}$ is observed at 0.478 MeV with a 6σ confidence level. For comparison, if one considers the transmission of γ -rays in the same energy range [25] propagating through 1/8 inch of Al, 8 cm of LiH, 5/8 inches of Pb (shielded LiH), and 1/8 inch of Al, 5/8 inch of Pb (shielding alone), the attenuation of γ -rays alone, under our experimental conditions, does not differ enough to detect the presence of LiH. This difference (5%) lies within the standard deviation of the background (27%) in our experiment. Moreover, only NRF provides a characteristic energy signature and isotopic sensitivity. In addition, simple calculations, using the known NRF cross section of ${}^7\text{Li}$ and x-ray NIST attenuation data [25], show that NRF becomes more effective as the Pb shielding increases.

Having detected NRF from ${}^7\text{Li}$, we investigated another method to ascertain the presence or absence of a given isotope that has the potential to yield lower false positive and negative rates [4]. In this method, first proposed by Bertozzi [26], γ -rays are transmitted through the material under interrogation to a reference sample containing the isotope of interest. If NRF is detected from the reference, one can conclude that the interrogated material did not contain the isotope. If no NRF is observed, either the resonant photons have been scattered by the isotope in the interrogated sample, or the material is optically too thick; the latter case can be ruled out by a simple transmission measurement. Since this method relies on the creation of a notch in the transmitted spectrum at the NRF energy by the isotope of interest, the advantages of narrow-band, highly collimated light sources are clear.

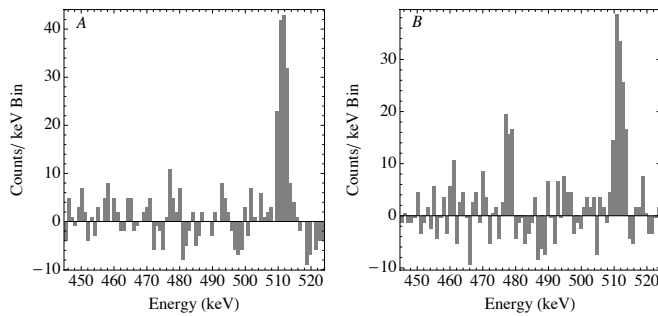


FIG. 4: NRF detection in ${}^7\text{Li}$ with two samples: output of reference detector when the interrogated LiH is (A) out of the beam (resonant photons present in the incident spectrum) and (B) in the beam (resonant photons absent from the incident spectrum).

We placed an identical test LiH sample in the beam path before the reference LiH bottle already present. It was mounted on a horizontal translation stage so that we could observe the effect on the NRF scattered spectrum in the reference sample. The data displayed in Fig. 4 represent the scattered spectra obtained the reference detector when the LiH is in and out of the beam, with background subtraction. In each spectrum the 511 keV line can be observed, as in Fig. 3. When the test sample is in the beam, the NRF line is not observed on the reference detector (Fig. 4A). When the LiH sample is pulled out, the NRF line appears on the reference detector (Fig. 4B).

In conclusion, we have shown that low-Z, low density material (${}^7\text{Li}$) can be detected behind high-Z, high density material (Pb) by using nuclear resonance fluorescence excited by a high-energy, high-brightness Compton scattering light source. Indeed, radiography frequently fails with heavily shielded low-Z objects because the low-energy portion of the Bremsstrahlung spectrum; i.e. the part of the spectrum that interacts most strongly with low-Z materials (thereby providing high image contrast) is often very strongly attenuated by the shielding. NRF probes (typically MeV scale) can easily penetrate modest amounts of shielding and still provide very high image contrast in hidden low-Z materials if there is a strong NRF resonant absorption. NRF provides unique isotope sensitivity and narrow-band, laser-based Compton sources are very well suited to NRF-based detection. The capability to observe optically thin objects embedded in optically thick material with deeply penetrating radiation has numerous potential applications ranging from medical imaging to homeland security, nuclear waste assay and stockpile stewardship.

This work was performed under the auspices of the U.S. Department of Energy by Lawrence Livermore National Laboratory under Contract DE-AC52-07NA27344. Additional support from the Domestic Nuclear Detection Organization (DNDO) from the Department of Homeland Defense is also acknowledged. The Authors wish to thank Gerry Anderson for the electron beam operations and detectors shielding, Shawn Betts for laser operations, as well as James Hall for very useful discussions on radiography.

-
- [1] G. Rennie, ST Review, Lawrence Livermore National Laboratory, March 2005.
- [2] C. Middleton, ST Review, Lawrence Livermore National Laboratory, December 2002.
- [3] A. Heller, ST Review, Lawrence Livermore National Laboratory, April 2004.
- [4] J. Pruet, D.P. McNabb, C.A. Hagmann, F.V. Hartemann and C.P.J. Barty, *J. Appl. Phys.*, 99, 123102 (2006)
- [5] U. Kneissl, H.M. Pitz and A. Zilges, *Prog. Part. Nucl. Phys.*, 37, pp 349-433 (1996)
- [6] W. Bertozzi, J.A. Caggiano, W.K. Hensley, M.S. Johnson, S.E. Korbly, R.J. Ledoux, D.P. McNabb, E.B. Norman, W.H. Park and G.A. Warren, *Phys. Rev. C*, 78, 041601(R) (2008)
- [7] F.V. Hartemann, W.J. Brown, D.J. Gibson, S.G. Anderson, A.M. Tremaine, P.T. Springer, A.J. Wootton, E.P. Hartouni and C.P.J. Barty, *Phys. Rev. ST Accel. Beams*, 8, 100702 (2005)
- [8] V.N. Litvinenko, *Nucl. Instr. Phys. Res. A*, 507, pp 527-536 (2003)
- [9] R. Schoenlein, W. Leemans, A. Chin, P. Volfbeyn, T. Glover, P. Balling, M. Zolotarev, M. Kim, S. Chattopadhyay, and C. Shank, *Science*, 274, 236 (1996)
- [10] F.V. Hartemann et al, *Las. Part. Beams*, 22, 221 (2004)
- [11] D.J. Gibson, S.G. Anderson, C.P.J. Barty, S.M. Betts, R. Booth, W.J. Brown, J.K. Crane, R.R. Cross, D.N. Fittinghoff, F.V. Hartemann, J. Kuba, G.P. Lesage, D.R. Slaughter, A.M. Tremaine, A.J. Wootton, E.P. Hartouni, P.T. Springer and J.B. Rosenzweig, *Phys. Plasmas*, 11, 2857 (2004)
- [12] W.D. Andrews, F.E. Carroll, J.W. Waters, C.A. Brau, R.H. Price, D.R. Pickens, P.A. Tompkins and C.F. Roos, *Nucl. Instr. Phys. Res. A*, 318, pp 189-196 (1992)
- [13] N. Kikuzawa et al., to be published
- [14] D.J. Gibson et al., submitted to *Phys. Rev. ST Accel. Beams* (2009)
- [15] J. W. Dawson, M. J. Messerly, H. H. Phan, J. K. Crane, R. J. Beach, C. W. Siders, and C.P.J. Barty, High-Energy, Short-Pulse Fiber Injection Lasers at Lawrence Livermore National Laboratory, *IEEE J. Selected Topics in Quantum Electronics* 15 207-219 (2009).
- [16] K. O. Hill, F. Bilodeau, B. Malo, T. Kitagawa, S. Thriault, D. C. Johnson, J. Albert, and K. Takiguchi, *Opt. Lett.* 19, 1314-1316 (1994).
- [17] C.W. Siders, J.L.W. Siders, A. J. Taylor, S-G Park and A.M. Weiner, *Appl. Optics*, 37, 5302 (1998)
- [18] D. Strickland and G. Mourou, *Opt. Commun.* 56,219 (1985).

- [19] D.N. Fittinghoff, W.A. Molander and C.P.J. Barty, "Hyperdispersion grating arrangements for compact pulse compressors and expanders", Oct 14, 2004, UCRL-CONF-203845.
- [20] W.J. Brown, S.G. Anderson, C.P.J. Barty, S.M. Betts, R. Booth, J.K. Crane, R.R. Cross, D.N. Fittinghoff, D.J. Gibson, F.V. Hartemann, E.P. Hartouni, J. Kuba, G.P. Le Sage, D.R. Slaughter, A.M. Tremaine, A.J. Wooton and P.T. Springer, Phys. Rev. ST Accel. Beams, 7, 060702 (2004)
- [21] R.A. Forster et al. NIMB 213, pp. 82-86 (2004)
- [22] F. Albert et al., submitted to Phys. Rev. ST Accel. Beams (2009)
- [23] N. Pietralla et al., Phys. Rev. Lett. 88, 012502 (2002)
- [24] L.W. Fagg and S.S. Hanna, Rev. Mod. Phys. 31, 711 (1959)
- [25] <http://www.nist.gov>
- [26] W. Bertozzi, S.E. Kobly, R.J. Ledoux and W. Park, Nucl. Instr. Phys. Res. B, 261, 331-336 (2007)